Influence of size-corrected bound-electron contribution on nanometric silver dielectric function. Sizing through optical extinction spectroscopy

2013 J. Phys. D: Appl. Phys. 46 435301

(http://iopscience.iop.org/0022-3727/46/43/435301)

J. Phys. D: Appl. Phys. **46** (2013) 435301 (10pp) doi:10.1088/0022-3727/46/43/435301

Influence of size-corrected bound-electron contribution on nanometric silver dielectric function. Sizing through optical extinction spectroscopy

J M J Santillán[1], F A Videla[1,2], M B Fernández van Raap[3], D Muraca[4], L B Scaffardi[1,2,5] and D C Schinca[1,2]

[1] Centro de Investigaciones Ópticas (CIOp), (CONICET La Plata-CIC), Argentina
[2] Departamento de Ciencias Básicas, Facultad de Ingeniería, UNLP, Argentina
[3] Instituto de Física La Plata (IFLP), Departamento de Física, Facultad de Ciencias Exactas, UNLP, CONICET, Argentina
[4] Instituto de Física 'Gleb Wataghin' (IFGW), Universidade Estadual de Campinas, Brazil

E-mail: lucias@ciop.unlp.edu.ar

Received 19 July 2013, in final form 28 August 2013
Published 1 October 2013
Online at stacks.iop.org/JPhysD/46/435301

Abstract
The study of metal nanoparticles (NPs) is of great interest due to their ability to enhance optical fields on the nanometric scale, which makes them interesting for various applications in several fields of science and technology. In particular, their optical properties depend on the dielectric function of the metal, its size, shape and surrounding environment.

This work analyses the contributions of free and bound electrons to the complex dielectric function of spherical silver NPs and their influence on the optical extinction spectra. The contribution of free electrons is usually corrected for particle size under 10 nm, introducing a modification of the damping constant to account for the extra collisions with the particle's boundary.

For the contribution of bound electrons, we considered the interband transitions from the d-band to the conduction band including the size dependence of the electronic density states for radii below 2 nm. Bearing in mind these specific modifications, it was possible to determine optical and band energy parameters by fitting the bulk complex dielectric function. The results obtained from the optimum fit are: $K_{\mathrm{bulk}} = 2 \times 10^{24}$ (coefficient for bound-electron contribution), $E_{\mathrm{g}} = 1.91$ eV (gap energy), $E_{\mathrm{F}} = 4.12$ eV (Fermi energy), and $\gamma_{\mathrm{b}} = 1.5 \times 10^{14}$ Hz (damping constant for bound electrons).

Based on this size-dependent dielectric function, extinction spectra of silver particles in the nanometric–subnanometric radius range can be calculated using Mie's theory, and its size behaviour analysed. These studies are applied to fit experimental extinction spectrum of very small spherical particles fabricated by fs laser ablation of a solid target in water. From the fitting, the structure and size distribution of core radius and shell thickness of the colloidal suspension could be determined. The spectroscopic results suggest that the colloidal suspension is composed by two types of structures: bare core and core–shell. The former is composed by Ag, while the latter is composed by two species: silver–silver oxide (Ag–Ag_2O) and hollow silver (air–Ag) particles. High-resolution transmission microscopy and atomic force microscopy analysis performed on the dried suspension agree with the sizing obtained by optical extinction spectroscopy, showing that the latter is a very good complementary technique to standard microscopy methods.

(Some figures may appear in colour only in the online journal)

[5] Author to whom any correspondence should be addressed. Also at: CIOp CC3 (1897) Gonnet, La Plata, Argentina.

1. Introduction

The control of material properties in the nanometric scale is based on the ability to manipulate size to extend the applications in different areas of research [1]. Silver nanoparticles (NPs) have very important applications in biomedical sciences as well as in technology due to their specific physical, chemical and biological properties.

In the area of biomedicine, silver NPs are being used as biosensors [2–5], as well as for treatment of diseases such as retinal neurovascularization [6, 7] and cancer [8–10]. A noticeable application of these NPs is related to their well-known bactericide properties. In this sense, they are used as antiviral agents against hepatitis B [11], HIV-1 [12, 13], monkeypox virus [14], herpes simplex virus type 1 [15], H1N1 influenza A virus [16–18], respiratory syncytial virus [19], among others. An interesting characteristic is the observed antiviral activity dependence on Ag NPs size. For example, Elechiguerra *et al* [12] concluded that NPs with radii smaller than 10 nm specifically inhibited infection by HIV-1.

In the field of technology, applications include optical switches [20], photovoltaic, optoelectronic and plasmonic devices [21–23], solar cells [24], high density optical data storage [25, 26], among others.

In particular, core–shell structured Ag NPs have attracted attention due to their capability to improve electrical and thermal conductivity properties in anisotropic conductive adhesives when they are incorporated as monolayer-coated silver NPs [27] or silver core–silver oxide nanoshells in silica nanocomposites [28].

Optical characterization of NPs through the study of their dielectric function and optical extinction spectra is important for applications in the mentioned areas. This, in turn, can be used to control their plasmonic properties. In recent studies we have shown a theoretical method related to the fit of the full UV–Vis experimental extinction spectra, which allows the characterization of metallic NPs such as gold, silver and copper with sizes below 20 nm using Mie's theory [29], together with a suitable modification of the bulk complex dielectric function for free and bound electrons [30–38]. In the contribution of free electrons, this modification is concerned with the damping constant in Drude's model, which increases due to collisions of electrons with the boundary of the particle, thus producing a size dependence in the dielectric function for NPs with radii between 2–10 nm. For the case of the contribution of bound electrons, the interband transitions of these electrons to conduction band levels contribute appreciably to the dielectric function for NPs' size smaller than 2 nm. In previous papers, we analysed the influence of free and bound electrons on the dielectric function and its dependence with size for gold and copper NPs [30, 35, 36]. However, for the case of silver NPs this has not been fully studied.

In this paper, we first study the size dependence on the complex dielectric function and then analyse its influence on the extinction spectra of silver NPs. The values of different parameters involved in the model are determined taking into account free and bound electrons contributions. Extinction spectra analysis is applied to sizing nanometric and subnanometric core–shell particles generated by femtosecond laser ablation in water. The spectrum fit reveals that Ag–Ag_2O and air–Ag core–shell NPs are present in the colloidal suspension.

2. Theoretical modelling for the metal dielectric function

The theoretical modelling of the total complex dielectric function for metals was extensively studied in previous works [30, 35, 36, 38, 39]. However, we will briefly overview the main concepts in the following paragraphs.

For bulk metals, the complex dielectric function can be decomposed into two contributions: a free-electron term and an interband (or bound-electron) term:

$$\varepsilon_{\text{bulk}}(\omega) = \varepsilon_{\text{free-electrons}}(\omega) + \varepsilon_{\text{bound-electrons}}(\omega). \tag{1}$$

For spherical NPs of size less than 10 nm radii, the complex free-electron contribution becomes dependent on the radius r and can be written as:

$$\varepsilon_{\text{free-electrons}}(\omega, r) = 1 - \frac{\omega_{\text{p}}^2}{\omega^2 + \text{i}\gamma_{\text{size}}(r)\omega}, \tag{2}$$

where $\omega_{\text{p}} = 13.8 \times 10^{15}$ Hz [40] is the silver bulk plasma frequency and $\gamma_{\text{size}}(r) = \gamma_{\text{bulk}} + C(\nu_{\text{F}}/r)$, the size dependent damping constant. In the last expression, $\gamma_{\text{bulk}} = 2.7 \times 10^{13}$ Hz [40] is the bulk damping constant in the Drudel model, $\nu_{\text{F}} = 14.1 \times 10^{14}\,\text{nm s}^{-1}$ [41] the Fermi velocity, r the particle radius and $C = 0.8$ a constant related to electron scattering processes within the particles, as derived from first-principles calculations [42].

For a complex dielectric function related to bound electrons contribution, we considered transitions from silver d-band to conduction band using the expression given by Bigot *et al* [43], which can be modified to take into account the increasing spacing of the energy levels when particle size decreases [30, 35, 36, 39]:

$$\varepsilon_{\text{bound-electrons}}(\omega, r) = K_{\text{size}}(r) \int_{\omega_{\text{g}}}^{\infty} \frac{\sqrt{x - \omega_{\text{g}}}}{x} \times [1 - F(x, T)] \frac{(x^2 - \omega^2 + \gamma_{\text{b}}^2 + \text{i}2\omega\gamma_{\text{b}})}{(x^2 - \omega^2 + \gamma_{\text{b}}^2)^2 + 4\omega^2\gamma_{\text{b}}^2}\,\text{d}x \tag{3}$$

being $\hbar\omega_{\text{g}}$ the gap energy (E_{g}); $F(x, T)$, the Fermi energy distribution function of conduction electrons with energy $\hbar x$ at temperature T for Fermi energy E_{F}. γ_{b} represents the damping constant in the interband transition and $K_{\text{size}}(r) = K_{\text{bulk}}(1 - \exp(-r/r_0))$ a radius-dependent proportionality factor [30, 35, 36, 39], where r is the particle radius, $r_0 = 0.35$ nm a scale factor and K_{bulk} a proportionality constant. $K_{\text{size}}(r)$ is introduced in equation (3) to take into account the size dependence of bound-electron contribution following the idea of Logunov *et al* [44], assuming that the electronic density of states is different for NPs of different size. Therefore, small particles have larger spacing range between electronic states, so the density of states will be smaller for very small NPs.

3. Optical extinction spectroscopy calculations

For NPs of size smaller than the incident wavelength, the response to optical extinction can be described with the electrostatic approximation of Mie theory. The expression for the general case of a spherical core–shell structure can be written as:

$$C_{\text{ext}} = k'\text{Im}(\alpha) = k'\text{Im} \times \left[4\pi r'^3 \frac{(\varepsilon_2 - \varepsilon_m)(\varepsilon_1 + 2\varepsilon_2) + f(\varepsilon_1 - \varepsilon_2)(\varepsilon_m + 2\varepsilon_2)}{(\varepsilon_2 + 2\varepsilon_m)(\varepsilon_1 + 2\varepsilon_2) + f(2\varepsilon_2 - 2\varepsilon_m)(\varepsilon_1 - \varepsilon_2)}\right], \quad (4)$$

where α is the polarizability, $k' = 2\pi n_m/\lambda$ and n_m are the wavenumber and refractive index of the surrounding medium, respectively, and λ the wavelength of the incident light in vacuum.

In the expression inside brackets, $f = (r/r')^3$ is the ratio between inner and outer volumes, with $r = r_{\text{core}}$ being the radius of the metal central core (silver) and $r' = r_{(\text{core+coating})}$ the outer radius (silver core + silver oxide shell thickness); $\varepsilon_1 = \varepsilon_1(\lambda, r)$, $\varepsilon_2 = \varepsilon_2(\lambda)$ and $\varepsilon_m = \varepsilon_m(\lambda)$ are the dielectric function of core, shell and surrounding medium, respectively.

For fitting purposes, we use the so called extinction coefficient, that is related to the extinction cross section (C_{ext}) through the equation $Q_{\text{ext}} = C_{\text{ext}}/\pi r'^2$.

4. Experimental section

Silver colloidal suspension was generated by fs laser ablation in water. The silver target sample used to conduct these experiments was a 1 mm thick high purity grade circular solid disc immersed in water. Laser ablation was accomplished using a Ti : Sapphire chirped pulsed amplification (CPA) system from Spectra Physics, emitting pulses of 100 fs width at 1 kHz repetition rate centred at 800 nm wavelength. This system produces fs pulses with energy up to 1 mJ per pulse. However, a classical waveplate-polarizer system has been employed for attenuation purposes. The laser beam was focused on the solid disc surface by a lens of 5 cm focal length. The energy per pulse was set at 500 μJ. The experimental setup chosen to produce silver NPs in liquid media is shown in figure 1.

The sample was placed over a programmable *XY* motorized micrometric stage, to produce suitable displacements so that the laser impinged always in a fresh area of the sample. This process lasted 9 min, after which the water showed a typical yellowish colour, attributed to the presence of a significant amount of silver particles in the liquid.

Optical extinction spectroscopy was implemented by means of a Shimadzu spectrophotometer from 300 to 1000 nm. For the samples analysed by optical extinction spectroscopy (OES) technique, surfactants additions to the solutions in order to avoid agglomeration effects were not needed. Colloidal suspension optical absorption measurements were performed 5 min after fabrication and further sonication. This *in situ* measurement prevents possible NPs coalescence and provides reliable statistics.

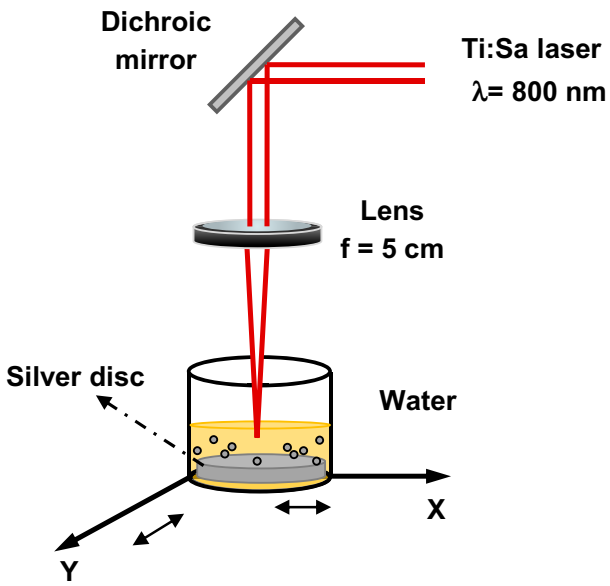

Figure 1. Schematic diagram of machining setup for the fabrication of silver colloidal suspension.

For atomic force microscopy (AFM) imaging, part of the as-prepared sample was diluted to ensure single particle observation. A drop of such diluted sample was placed on a freshly cleaved muscovite mica sheet V-1 grade (SPI Supplies) and dried for 40 min in an oven at 42 °C. The analysis of mica sheet measurement indicates an average roughness of 0.0612 nm.

Images were recorded in air, at room temperature, and at a scan rate of 1 Hz, using standard semicontact AFM mode. NT-MDT Solver Pro equipped with a APPNANO-ACTA silicon probe consistent for high-resolution imaging was used.

The rectangular cantilever of 40 N m^{-1} force constant and 281.8 kHz resonant frequency holds a sharp tip of 6 nm curvature radius. Minimum scanning step in vertical direction is 0.012 nm.

Transmission electron microscopy imaging was carried out with a TEM-MSC (JEOL 2100) at Brazilian Synchrotron Light Laboratory (LNLS). The particles were dispersed on milli-Q water and sonicated for 15 min. Samples were obtained by drying the water-dispersed NPs on a carbon-coated copper grid and images were acquired with the sample on a single-tilt sample holder and a TV Gatan ES500W camera.

5. Theoretical fitting and experimental results

The general form for the metal NP complex dielectric function is obtained by introducing the expressions (2) and (3) in equation (1), taking into account the specific modifications for $\gamma_{\text{size}}(r)$ and $K_{\text{size}}(r)$. With the dielectric function written in this way, it is possible to fit the experimental bulk dielectric function measured by Johnson and Christy [40], considering $r = 100$ nm ($r \gg r_0$). This simultaneous fitting procedure of the real and imaginary parts of the dielectric constant allows determining optimum values for silver K_{bulk}, E_g, E_F and γ_b, which are shown in table 1. These physical magnitudes were

Table 1. Optical and band energy parameters for bulk silver determined in this work.

Silver parameter	Symbol	Value
Bound-electron coefficient	K_{bulk}	2×10^{24}
Gap energy	E_{g}	1.91 eV
Fermi energy	E_{F}	4.12 eV
Bound-electron damping constant	γ_{b}	1.5×10^{14} Hz

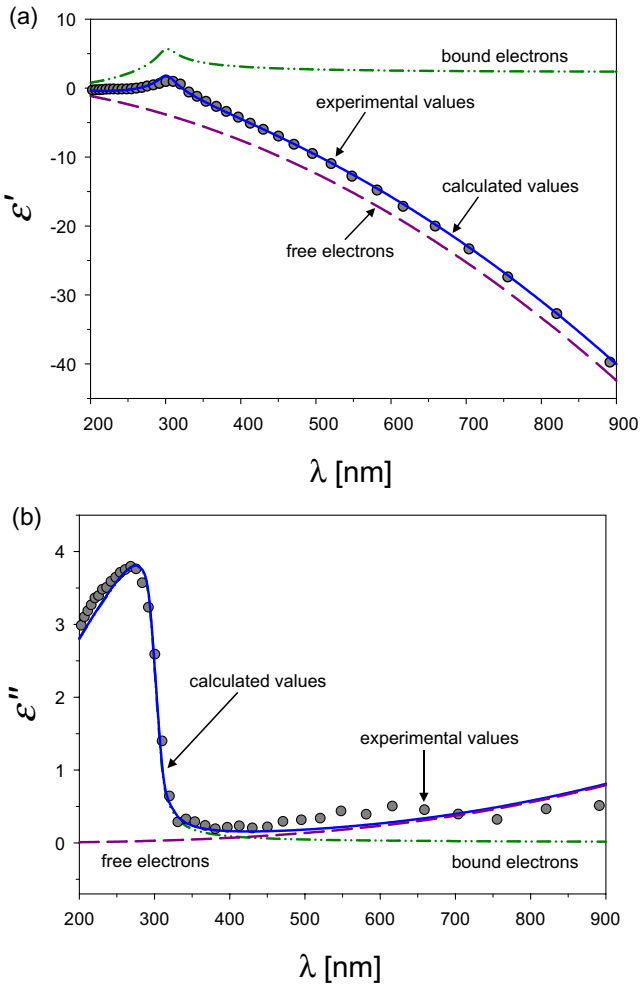

Figure 2. Free and bound electrons contribution to the real (*a*) and imaginary (*b*) parts of silver dielectric function calculated with equations (2) and (3). Experimental values are fitted through the theoretical model explained in the text.

determined for the first time with this kind of spectroscopic method. In particular, K_{bulk} and γ_{b} were determined for the first time to the best of our knowledge.

Figure 2 shows the real (*a*) and imaginary part (*b*) of the experimental dielectric function (full circles) taken from Johnson and Christy [40], together with free (dashed line) and bound (dashed line and dots) electron contributions calculated with equations (2) and (3), respectively, that best fits the experimental data (full line).

It is interesting to observe that bound-electron contribution in figure 2(*b*) presents a dominant behaviour for wavelengths smaller than 400 nm, while free electrons show a stronger contribution for wavelengths larger than 400 nm. The fit of

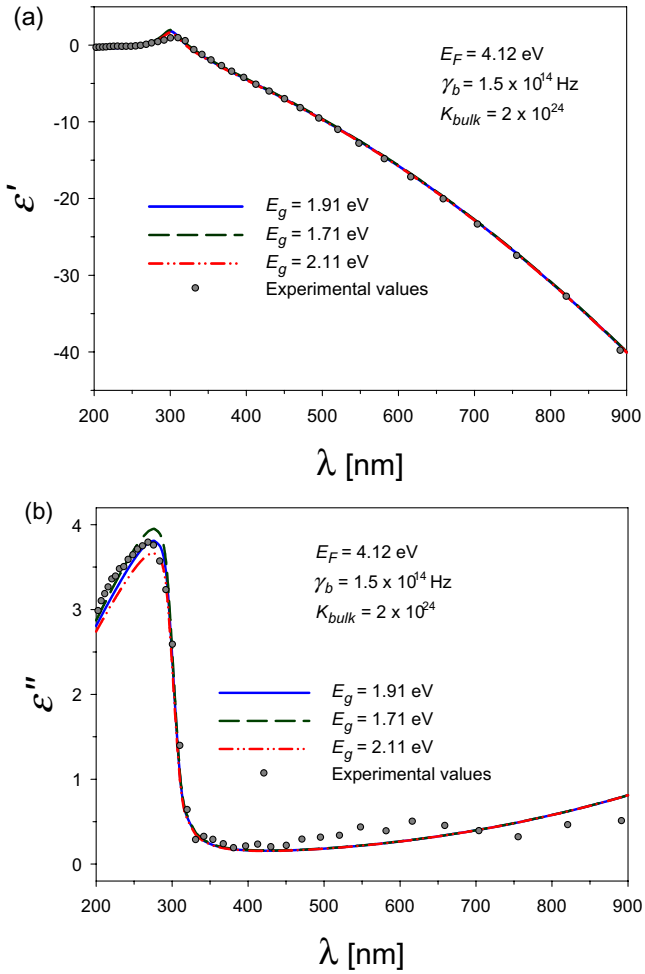

Figure 3. E_{g} influence on bulk complex dielectric function of silver: (*a*) real part and (*b*) imaginary part.

both the real and imaginary part is very good considering the different scale lengths of the graphs (about one order of magnitude). It also has to be taken into consideration that, since the imaginary part is related to absorption transitions, it poses some difficulties in its experimental measurement, probably inducing a larger error dispersion than the real part.

The obtained values for E_{F} and E_{g} agree, within experimental errors, with those obtained by other authors and methods [45]. To analyse the sensitivity of the bulk complex dielectric function curves to variations of these parameters, modifications in the shape of the curves due to small changes in the values of E_{g}, E_{F} and γ_{b} are shown in figures 3 to 5, respectively.

The influence of E_{g} on the complex dielectric function can be observed in figures 3(*a*) and (*b*). Changes in the imaginary part (figure 3(*b*)) are more noticeable for wavelengths smaller than 290 nm.

On the other hand, figures 4(*a*) and (*b*) allows observing the influence of E_{F} on the complex dielectric function. Figure 4(*b*) shows the shift produced on the steep slope of the imaginary part between 270 and 340 nm.

The behaviour of silver bulk complex dielectric function for different values of γ_{b} is represented in figures 5(*a*) and (*b*).

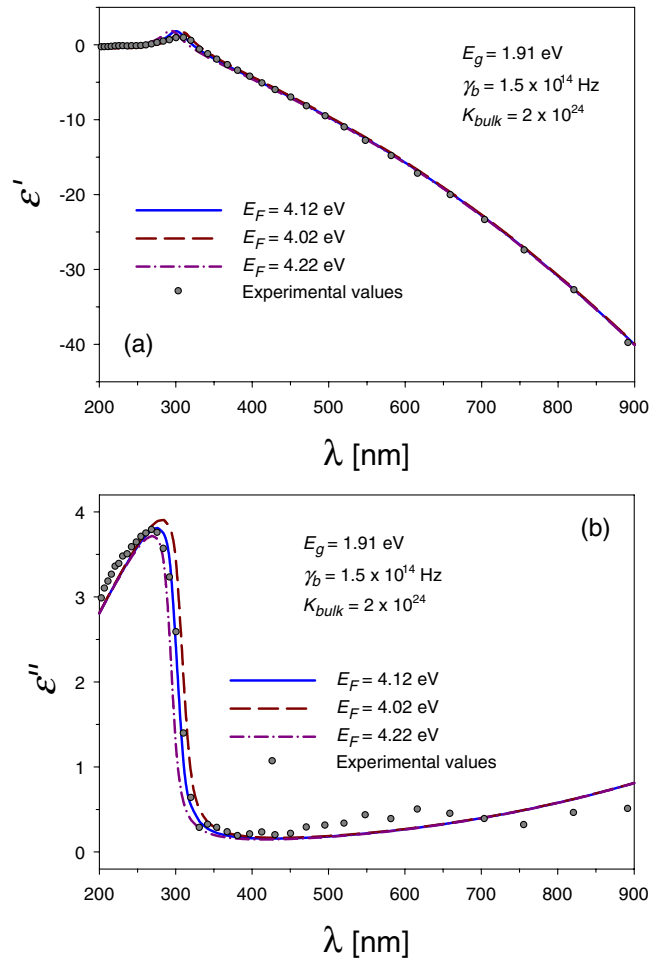

Figure 4. Influence of E_F on the bulk complex dielectric function of silver: (*a*) real and (*b*) imaginary component.

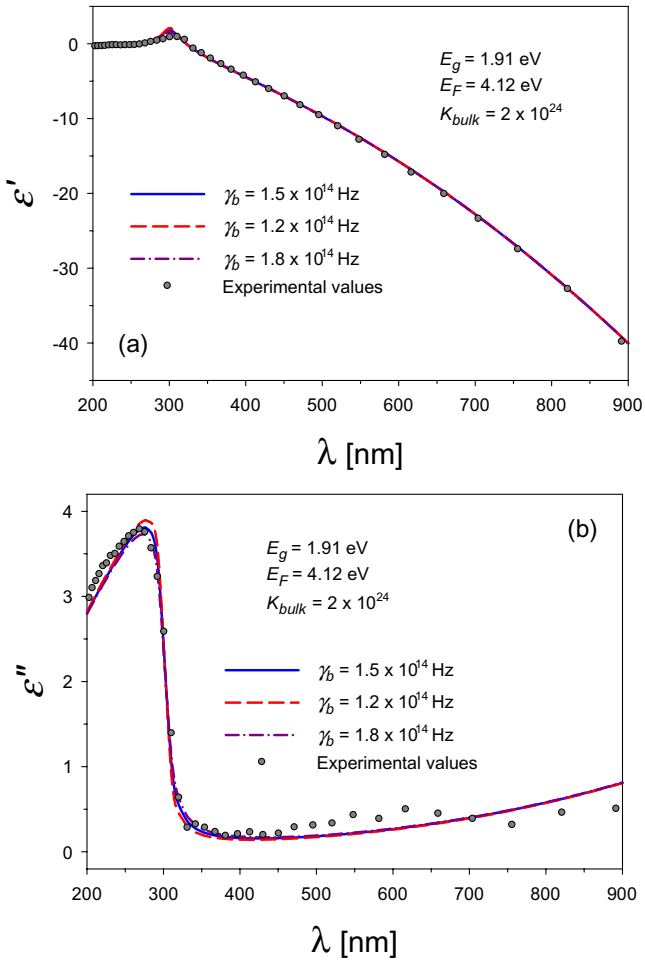

Figure 5. Influence of γ_b on the bulk complex dielectric function of silver: (*a*) real and (*b*) imaginary component.

Figure 5(*b*) shows small variations around 280 and 340 nm (peak and valley, respectively).

Considering the independent influence of these parameters over different dielectric function wavelength range, it was possible to use them to fit the experimental bulk dielectric function and to obtain the optimum values shown in table 1. Once these bulk parameters are known, we can analyse the theoretical behaviour of the contribution of free and bound electrons to the silver complex dielectric function for different radii.

Figures 6(*a*) and (*b*) shows the real and imaginary parts of the free electrons contribution to the dielectric function for several particle radii. It can be seen that the curves rapidly tend to bulk behaviour for sizes approaching 10 nm. The imaginary part plotted in figure 6(*a*) presents a limit behaviour for $r > 20$ nm, but there also seems to be a lower limiting behaviour for $r = 0.6$ nm.

Figure 7 shows the behaviour of real (*a*) and imaginary (*b*) parts of bound electrons contribution for different particles sizes. Figure 7(*a*) shows that the curves are very sensitive to small changes for radii under 1.5 nm at wavelengths larger than 300 nm, while for the imaginary part this sensitivity is more noticeable for wavelengths smaller than 300 nm. Anyway, in both cases bound electrons correction is negligible for sizes larger than 2 nm.

After analysing the behaviour of the free and bound electrons contribution to the dielectric function with the size in a nanometric–subnanometric radius range, it is possible to study the influence of size corrections in the extinction spectra.

Depending on laser ablation process parameters and on the environment, the fabricated silver NPs may be covered by a thin layer of silver oxide. This situation generates a silver–silver oxide core–shell structure showing optical extinction properties very different from those corresponding to silver bare core NPs.

Figure 8(*a*) shows the extinction coefficient for a Ag–Ag_2O particle for a subnanometric metal radius $r = 0.7$ nm covered by a thin layer of Ag_2O $r' - r = 0.35$ nm, in aqueous medium, calculated with and without bound-electron size correction. Silver oxide experimental dielectric function taken from Qiu *et al* [46] is plotted in the inset of the figure. It can be seen that the peak position is at about 485 nm for both spectra, while differences are more evident for wavelengths smaller than 520 nm, where the influence of the imaginary part of bound electrons is more important, while for wavelengths larger than 520 nm the spectra are coincident.

Figure 8(*b*) represents the extinction coefficient for a subnanometric silver bare core particle, which is a special case of core–shell particle where $r' = r$. There is an apparent

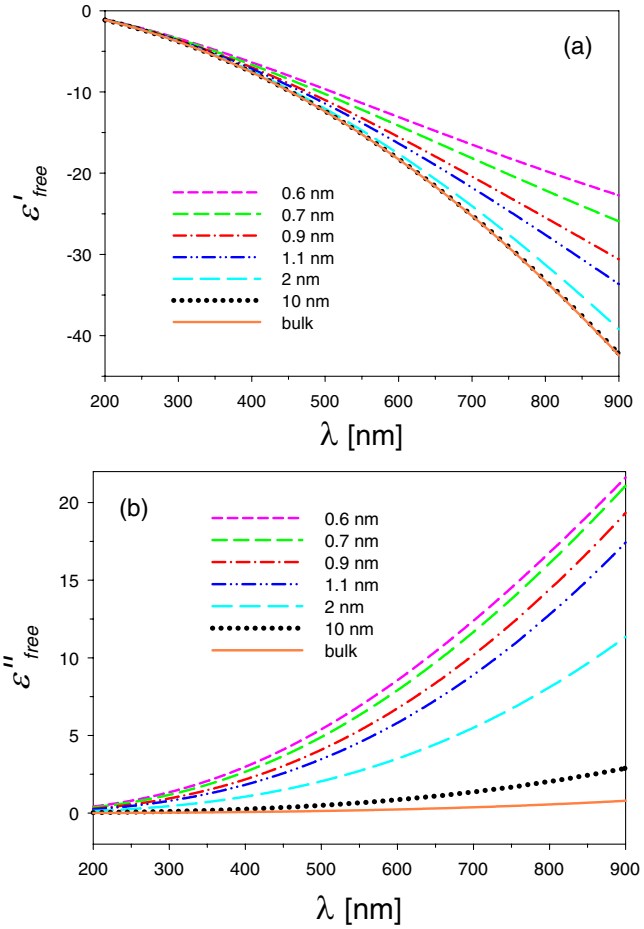

Figure 6. Real (*a*) and imaginary (*b*) parts of free electrons contribution to silver dielectric function calculated for several sizes. Full line represents bulk values.

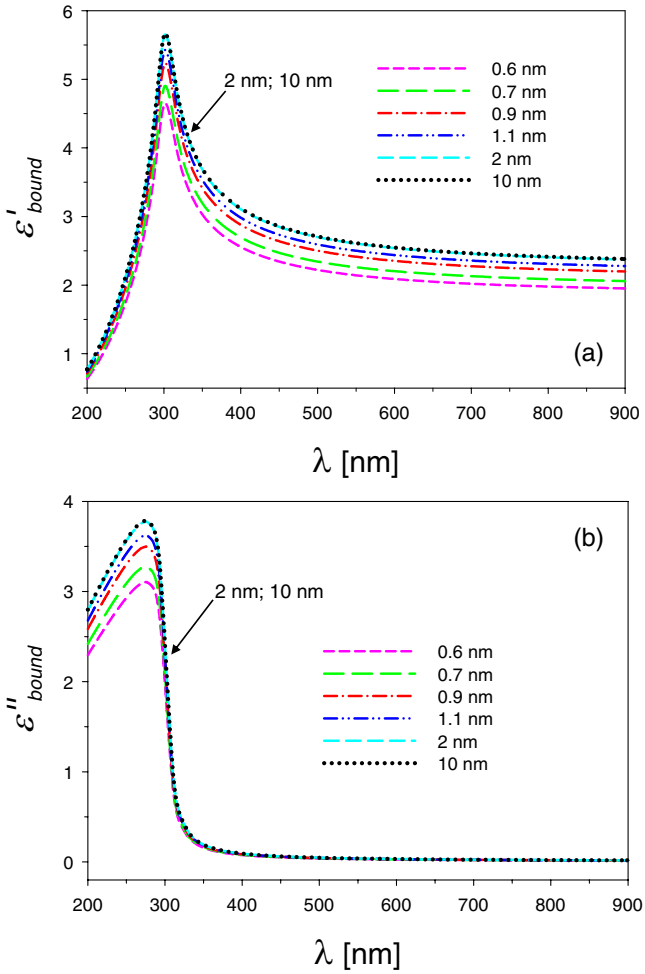

Figure 7. Real (*a*) and imaginary (*b*) components of bound electrons contribution to silver dielectric function calculated for different sizes.

discrepancy between the spectra for wavelengths lower than 400 nm. Plasmon resonance of a particle with the correction of bound electrons is at 375 nm, while without correction it is at 385 nm. On the other hand, theoretical calculation performed taking into account size correction, shows that the plasmon resonance is shifted to 485 nm (with oxide shell) with respect to the sharp peak at 375 nm when a particle without shell is considered.

For the full fit of the extinction spectrum, especially in the long wavelength range, it is necessary to include a hollow Ag NPs species. This kind of hollow core–shell NPs has been reported by other authors. For example, Desarkar *et al* [47], using laser ablation on zinc, obtained Zn/ZnO hollow NPs in liquids. Ben Moshe *et al* [48] produced colloidal hollow silver NPs by a fast chemical reduction of silver oxide NPs capped with glutathione, while Selvakannan and Sastry [49] produced hollow gold and platinum shell NPs through transmetallation reaction between hydrophobized silver NPs with hydrophobized chloroaurate and hydrophobized chloroplatinate ions in chloroform, respectively.

Taking into account these results, it was possible to analyse theoretically the behaviour of the hollow silver NPs extinction spectra. Figure 9 shows the extinction coefficient for an air–Ag NP immersed in water, with $r = 1$ nm radius covered by a subnanometric layer of Ag ($r' - r = 0.6$ nm), calculated with and without bound-electron size correction. It can be observed that the curve calculated with bound-electron size correction presents a larger contrast between peak and valley with respect to the curve calculated without size correction.

Taking into account the theoretical calculations for different species of spherical NPs (Ag bare core, Ag–Ag_2O or air–Ag core–shell), it was possible to fit the experimental extinction spectrum of the generated suspension. Figure 10 shows the best fit of the normalized experimental extinction spectrum corresponding to a colloidal suspension fabricated by fs laser ablation with 500 μJ pulse energy. This fit was attained considering two types of structures: bare core and core–shell. The former consists of bare core Ag NPs, while the latter contains two species of core–shell: Ag–Ag_2O and air–Ag NPs. Considering these types of structures, the optimum distribution that fits the experimental spectrum is composed by Ag–Ag_2O NPs with a dominant (relative abundance 72%) 2 nm core radius and 5.5% shell thickness, air–Ag NPs (relative abundance 24%) with an important contribution of 2 nm core radius and different shell thickness, together with bare Ag NPs of 2 nm radius (relative abundance 4%). This distribution can be observed in the inset of figure 10.

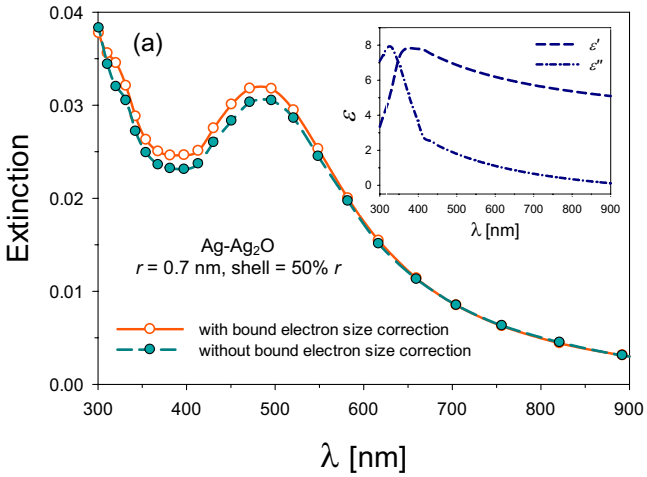

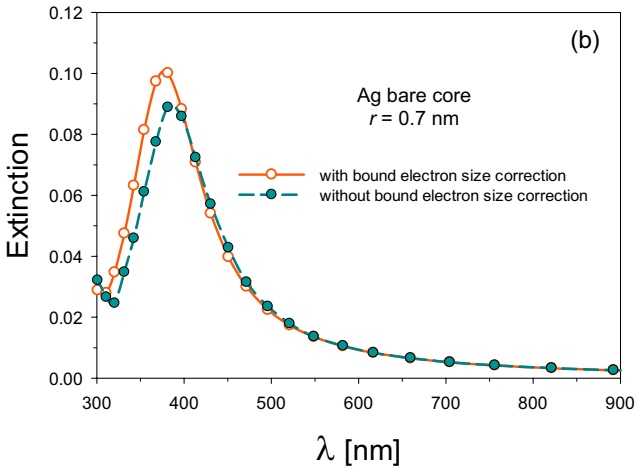

Figure 8. Extinction spectra for (*a*) core–shell Ag–Ag_2O NP and (*b*) subnanometric Ag bare core particle, with and without bound-electron size correction.

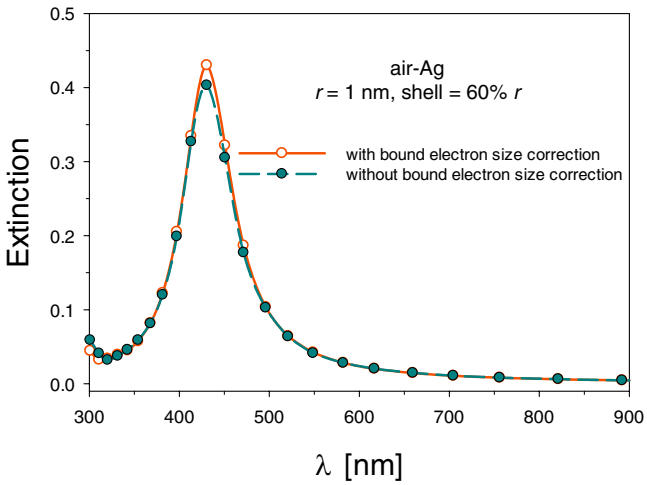

Figure 9. Extinction spectra for core–shell air–Ag NP with and without bound-electron size correction.

To compare sizing results obtained with OES method, we performed studies using AFM and high-resolution transmission microscope (HRTEM) of the same colloidal suspension. Figure 11(*a*) shows the AFM image of a 7 μm by 7 μm area, where spherical shape NPs can be seen,

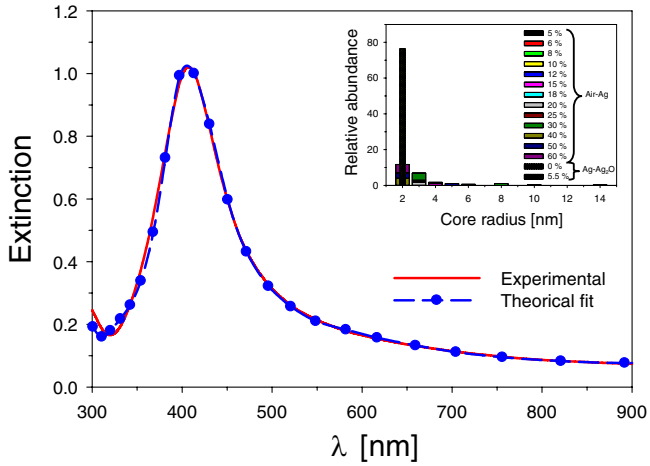

Figure 10. Experimental extinction spectrum of silver colloidal suspension generated in water with 500 μJ pulse energy. Theoretical fit was obtained with Ag–Ag_2O, air–Ag and bare core Ag NPs. Inset shows optimum size distribution of core radii and shell thickness that fits the experimental spectrum.

thus supporting the use of Mie approach for calculating the polarizability and the extinction spectrum. Several scans along selected NPs (dashed lines) were performed measuring the NPs' height (diameter) as well as surrounding substrate roughness. Figure 11(*b*) shows the profile of eleven lines scanned in the AFM image. Individual particle size is accurately retrieved. The registered heights are in agreement with the external radii distribution determined from the fit of the extinction spectrum of the sample. For these small size values, it is important to consider that the roughness of mica substrate (represented by the baseline profile) on which a sample drop was deposited is more than one order of magnitude smaller than the smallest recorded particle, ensuring a very good signal-to-noise ratio in the NP's profile.

Figure 12(*a*) shows the HRTEM image of the silver colloidal core–shell NPs obtained by fs pulse laser ablation. The sample dilution on milli-Q water was enough to allow single particle observation. It can be observed that the NPs are spherical, and in some cases, due to the sample preparation method, it is possible to observe unwanted coalescence effects. The typical sizes observed are in agreement with the results provided by extinction spectroscopy and AFM microscopy.

HRTEM image of these nanocrystals show distinct lattice fringe patterns (figure 12(*b*)), evidencing the highly crystalline nature of the nanocrystals. The lattice spacing obtained from the micrograph is 0.22 nm, which matches well to the (1 1 1) plane for the face-centred-cubic (fcc) crystal structure of bulk silver, as reported by Guascito *et al* [50].

6. Conclusions

This work was devoted to the theoretical modelling of complex silver dielectric function and to the characterization of size and structure of silver NPs colloidal suspension generated by ultrashort pulse laser ablation.

We have separately analysed the behaviour of free and bound electrons contributions to size-dependent complex dielectric function of silver NPs. Free electrons contribution

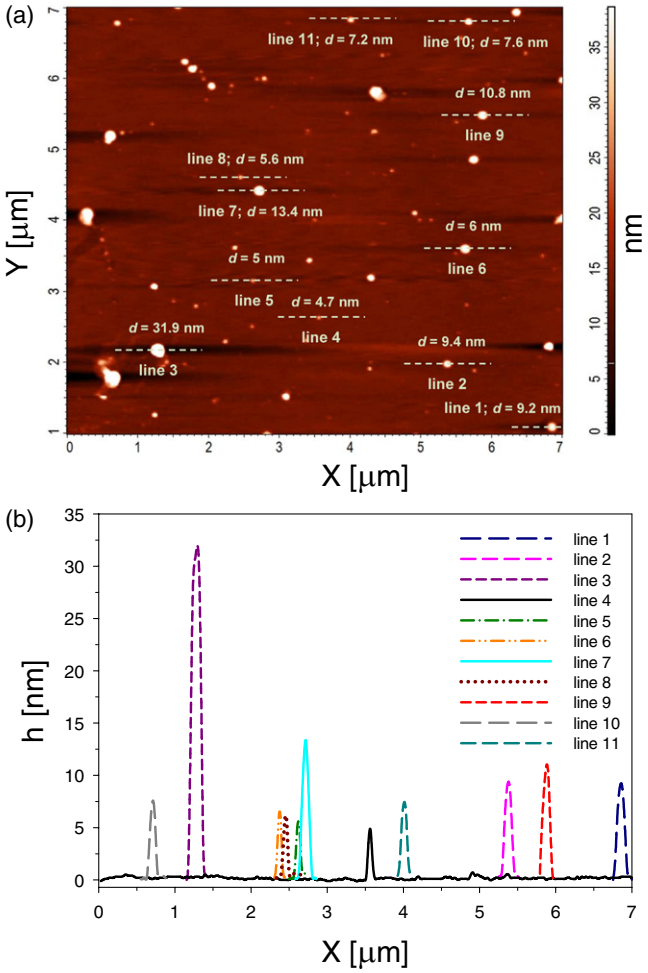

Figure 11. (*a*) AFM image of silver colloidal suspension generated in water with 500 μJ pulse energy, (*b*) height profiles of the eleven horizontal lines shown in (*a*).

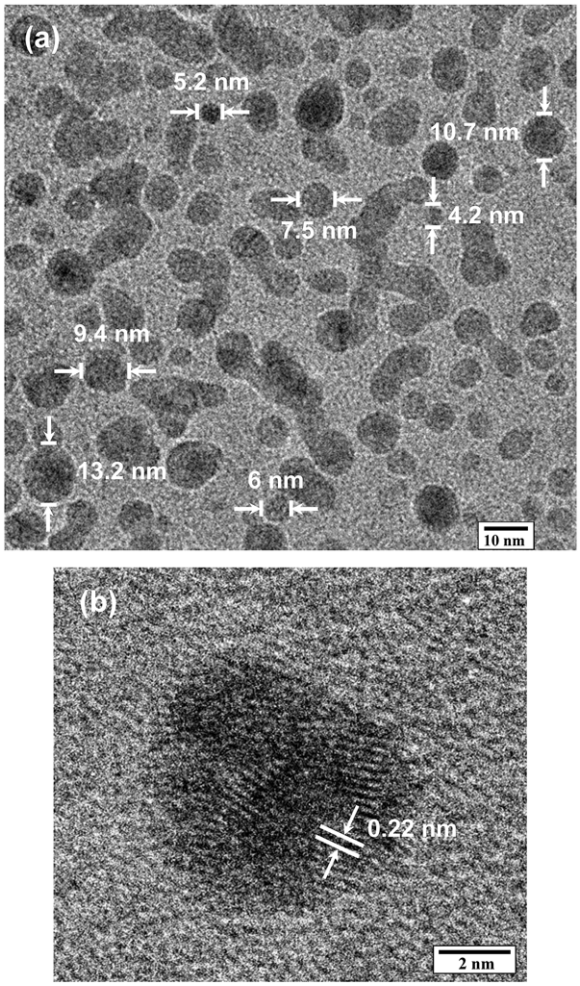

Figure 12. (*a*) HRTEM image of silver colloidal suspension fabricated in water with 500 μJ pulse energy; (*b*) separation of the Bragg planes for an isolated bare Ag NP of the same colloidal suspension.

was corrected for particle size as usual through a term inversely proportional to the particle radius in the expression of the bulk damping constant. With this correction, both real and imaginary parts of the free-electron contribution present an important dependence with size from 0.6 to 10 nm, with a limiting behaviour to bulk for a radius $r \approx 10$ nm. Bound electrons contribution based on transitions from d-band to conduction band were taken into account using an expression that considers all possible interband transitions at the band maximum without momentum change. The parameters involved in the expression for bulk bound electrons contribution, such as K_{bulk}, E_{g}, E_{F}, and γ_{b}, were determined by a simultaneous fit of the real and imaginary experimental values for bulk complex dielectric function of silver taken from Johnson and Christy [40]. For subnanometric particles, a radius-dependent proportionality factor that represents the increasing energy level spacing was included in the former expression for bound electrons dielectric function. This modification is important for radii up to about 2 nm, above which the correction is negligible.

The expression of the size-dependent complex dielectric function was used to calculate the polarizability involved in Mie's theory, showing the influence of bound electrons size modification on the extinction spectrum for subnanometric particles. It is interesting to point out that this approach is different from that frequently used in FDTD simulations [51, 52], where the bulk dielectric function is taken as an expansion of Lorentzian terms. Its parametrization is accomplished by determining the fitting parameters in the series expansion, using the resulting time-domain analytical function for simulation of optical properties of NPs. As stated above, the dielectric function in our work is built considering the band structure through a continuum of intra- and interband transitions which, finally, is made size-dependent for nanometric and subnanometric radii. In this case, the parametrization through a series expansion should include a term dependent on size.

For the case of Ag–Ag_2O NPs, the differences between the spectra with and without size correction are more significant for wavelengths smaller than 520 nm. For subnanometric Ag bare core particles, there is a noticeable difference between the spectra for wavelengths smaller than 400 nm, where the influence of the imaginary part of bound electrons is more important.

Considering this dielectric function model, we have successfully fitted the experimental extinction spectrum of

silver colloidal suspension generated by ultrashort pulse laser ablation (500 μJ pulse energy) of solid target in water. The obtained NPs are spherical and small in size (less than 15 nm radius), thus enabling the fit of the extinction spectrum using the electrostatic approximation of Mie theory. For the correct fit of the peak position and full spectrum, it was necessary to consider two types of core–shell NPs: Ag–Ag_2O and air–Ag. It was not possible to find a set of parameters that could fit the full spectrum considering only Ag bare core NPs.

The colloidal suspension sample was independently studied through AFM and HRTEM analysis. The results show very good agreement with those obtained from the fit of the experimental extinction spectra using the Drude-interband model.

Summarizing, OES can be applied thus as a complementary method to advanced microscopy techniques for sizing spherical bare core and core–shell NPs of the metal colloidal suspensions in the nanometer–subnanometer size range. OES allows determining structure (bare core or core–shell), structure type (Ag–Ag_2O or air–Ag) and relative abundance of NPs present in a colloidal suspension. It also has the advantage of providing very good measurement statistics due to the large number of particles in the path of the spectrophotometer beam across the sample cell. Besides, it avoids coalescence effects since the measurement is made directly on the colloidal suspension.

Acknowledgments

This work was performed by grants PIP (CONICET) 0394, PME 2006-00018 (ANPCyT), 11/I151 (Facultad de Ingeniería, Universidad Nacional de La Plata). AFM was performed at LFAyM of IFLP-CONICET, Argentina. D Muraca thanks FAPESP and C2NANO-Center for Nanoscience and Nanotechnology/MCT (# 13872) for the use of MSC-TEM equipment. D C Schinca and F A Videla are members of Comisión de Investigaciones Científicas de la Provincia de Buenos Aires (CIC). L B Scaffardi and M B Fernández van Raap are researchers of CONICET, and J M J Santillán is postdoc fellow of CONICET, Argentina.

References

[1] Bönnemann H and Richards R M 2001 Nanoscopic metal particles—Synthetic methods and potential applications *Eur. J. Inorg. Chem.* **10** 2455–80

[2] Haes A J and Van Duyne R P 2002 A nanoscale optical biosensor: sensitivity and selectivity of an approach based on the localized surface plasmon resonance spectroscopy of triangular silver nanoparticles *J. Am. Chem. Soc.* **124** 10596–604

[3] Riboh J C, Haes A J, McFarland A D, Yonzon C R and Van Duyne R P 2003 A nanoscale optical biosensor: real-time immunoassay in physiological buffer enabled by improved nanoparticle adhesion *J. Phys. Chem.* B **107** 1772–80

[4] Nam J M, Thaxton C S and Mirkin C A 2003 Nanoparticle-based bio-bar codes for the ultrasensitive detection of proteins *Science* **301** 1884–6

[5] Anker J N, Paige Hall W, Lyandres O, Shah N C, Zhao J and Van Duyne R P 2008 Biosensing with plasmonic nanosensors *Nature Mater.* **7** 442–53

[6] Bhattacharya R and Mukherjee P 2008 Biological properties of 'naked' metal nanoparticles *Adv. Drug Deliv. Rev.* **60** 1289–306

[7] Kalishwaralal K, BarathManiKanth S, Pandian S R K, Deepak V and Gurunathan S 2010 Silver nano—A trove for retinal therapies *J. Control. Release* **145** 76–90

[8] Vaidyanathan R, Kalishwaralal K, Gopalram S and Gurunathan S 2009 Nanosilver—the burgeoning therapeutic molecule and its green synthesis *Biotechnol. Adv.* **27** 924–37

[9] Moaddab S, Ahari H, Shahbazzadeh D, Motallebi A A, Anvar A A, Rahman-Nya J and Shokrgozar M R 2011 Toxicity study of nanosilver (nanocid®) on osteoblast cancer cell line *Int. Nano Lett.* **1** 11–16

[10] Govender R, Phulukdaree A, Gengan R M, Anand K and Chuturgoon A A 2013 Silver nanoparticles of Albizia adianthifolia: the induction of apoptosis in human lung carcinoma cell line *J. Nanobiotechnol.* **11** 1–9

[11] Lu L, Sun R W Y, Chen R, Hui C K, Ho C M, Luk J M, Lau G K K and Che C M 2008 Silver nanoparticles inhibit hepatitis B virus replication *Antivir. Ther.* **13** 253–62

[12] Elechiguerra J L, Burt J L, Morones J R, Camacho-Bragado A, Gao X, Lara H H and Yacaman M J 2005 Interaction of silver nanoparticles with HIV-1 *J. Nanobiotechnol.* **3** 1–10

[13] Lara H H, Ayala Nuñez N V, Ixtepan Turrent L and Rodriguez Padilla C 2010 Mode of antiviral action of silver nanoparticles against HIV-1 *J. Nanobiotechnol.* **8** 1–10

[14] Rogers J V, Parkinson C V, Choi Y W, Speshock J L and Hussain S M 2008 A preliminary assessment of silver nanoparticle inhibition of monkeypox virus plaque formation *Nanoscale Res. Lett.* **3** 129–33

[15] Baram Pinto D, Shukla S, Perkas N, Gedanken A and Sarid R 2009 Inhibition of herpes simplex virus type 1 infection by silver nanoparticles capped with mercaptoethane sulfonate *Bioconjug. Chem.* **20** 1497–502

[16] Mehrbod P, Motamed N, Tabatabaian M, Soleimani Estyar R, Amini E, Shahidi M and Kheiri M T 2009 In vitro antiviral effect of 'nanosilver' on influenza virus *DARU J. Pharm. Sci.* **17** 88–93

[17] Xiang D X, Chen Q, Pang L and Zheng C L 2011 Inhibitory effects of silver nanoparticles on H1N1 influenza A virus in vitro *J. Virol. Methods* **178** 137–42

[18] Mori Y, Ono T, Miyahira Y, Nguyen V Q, Matsui T and Ishihara M 2013 Antiviral activity of silver nanoparticle/chitosan composites against H1N1 influenza A virus *Nanoscale Res. Lett.* **8** 1–6

[19] Sun L, Singh A K, Vig K, Pillai S R and Singh S R 2008 Silver nanoparticles inhibit replication of respiratory syncytial virus *J. Biomed. Nanotechnol.* **4** 149–58

[20] Weiping C, Ming T and Lide Z 1996 Characterization and the optical switching phenomenon of porous silica dispersed with silver nano-particles within its pores *J. Phys.: Condens. Matter* **8** L591–6

[21] Wang D H, Park K H, Seo J H, Seifter J, Jeon J H, Kim J K, Park J H, Park O O and Heeger A J 2011 Enhanced power conversion efficiency in PCDTBT/PC_{70}BM bulk heterojunction photovoltaic devices with embedded silver nanoparticle clusters *Adv. Energy Mater.* **1** 766–70

[22] Maier S A, Kik P G, Atwater H A, Meltzer S, Harel E, Koel B E and Requicha A A G 2003 Local detection of electromagnetic energy transport below the diffraction limit in metal nanoparticle plasmon waveguides *Nature Mater.* **2** 229–32

[23] Zou S L and Schatz G C 2006 Metal nanoparticle array waveguides: proposed structures for subwavelength devices *Phys. Rev.* B **74** 125111–5

[24] Kalfagiannis N, Karagiannidis P G, Pitsalidis C, Panagiotopoulos N T, Gravalidis C, Kassavetis S, Patsalas P and Logothetidis S 2012 Plasmonic silver nanoparticles for improved organic solar cells *Sol. Energy Mater. Sol. Cells* **104** 165–74
[25] Peyser L A, Vinson A E, Bartko A P and Dickson R M 2001 Photoactivated fluorescence from individual silver nanoclusters *Science* **291** 103–6
[26] Tominaga J 2003 The application of silver oxide thin films to plasmon photonic devices *J. Phys.: Condens. Matter* **15** R1101–22
[27] Li Y, Moon K S and Wong C P 2005 Monolayer-protected silver nano-particle-based anisotropic conductive adhesives: enhancement of electrical and thermal properties *J. Electron. Mater.* **34** 1573–8
[28] Chatterjee K, Banerjee S and Chakravorty D 2002 Plasmon resonance shifts in oxide-coated silver nanoparticles *Phys. Rev.* B **66** 085421
[29] Bohren C F and Huffman D R 1998 *Absorption and Scattering of Light by Small Particles* (New York: Wiley)
[30] Scaffardi L B and Tocho J O 2006 Size dependence of refractive index of gold nanoparticles *Nanotechnology* **17** 1309–15
[31] Roldán M V, Scaffardi L B, de Sanctis O and Pellegri N 2008 Optical properties and extinction spectroscopy to characterize the synthesis of amine capped silver nanoparticles *Mater. Chem. Phys.* **112** 984–90
[32] Schinca D C and Scaffardi L B 2008 Core and shell sizing of small silver-coated nanospheres by optical extinction spectroscopy *Nanotechnology* **19** 495712–8
[33] Schinca D C, Scaffardi L B, Videla F A, Torchia G A, Moreno P and Roso L 2009 Silver–silver oxide core–shell nanoparticles by femtosecond laser ablation: core and shell sizing by extinction spectroscopy *J. Phys. D: Appl. Phys.* **42** 215102–9
[34] Santillán J M J, Scaffardi L B and Schinca D C 2011 Quantitative optical extinction-based parametric method for sizing a single core–shell Ag–Ag_2O nanoparticle *J. Phys. D: Appl. Phys.* **44** 105104–8
[35] Santillán J M J, Videla F A, Scaffardi L B and Schinca D C 2012 Plasmon spectroscopy for subnanometric copper particles: dielectric function and core–shell sizing *Plasmonics* **8** 341–8
[36] Santillán J M J, Videla F A, Fernández van Raap M B, Schinca D C and Scaffardi L B 2012 Size dependent Cu dielectric function for plasmon spectroscopy: characterization of colloidal suspension generated by fs laser ablation *J. Appl. Phys.* **112** 054319–8
[37] Santillán J M J, Videla F A, Schinca D C and Scaffardi L B 2012 Plasmonic properties and sizing of core–shell Cu–Cu_2O nanoparticles fabricated by femtosecond laser ablation in liquids *Plasmonics: Metallic Nanostructures and Their Optical Properties X Proc. SPIE* **8457** 84572U–8
[38] Santillán J M J, Videla F A, Fernández van Raap M B, Schinca D C and Scaffardi L B 2013 Analysis of the structure, configuration and sizing of Cu and Cu oxide nanoparticles generated by fs laser of solid target in liquids *J. Appl. Phys.* **113** 134305–9
[39] Scaffardi L B, Schinca D C, Lester M, Videla F A, Santillán J M J and Abraham Ekeroth R M 2013 Size-dependent optical properties of metallic nanostructures in: kumar *UV–VIS and Photoluminescence Spectroscopy for Nanomaterials Characterization* ed S S R Challa (Heidelberg: Springer) 179–229
[40] Johnson P B and Christy R W 1972 Optical constants of the noble metals *Phys. Rev.* B **6** 4370–9
[41] Kittel C 2007 *Introduction to Solid State Physics* (New York: Wiley)
[42] Kreibig U and Vollmer M 1995 *Optical Properties of Metal Clusters* (Berlin: Springer)
[43] Bigot J Y, Halté V, Merle J C and Daunois A 2000 Electron dynamics in metallic nanoparticles *Chem. Phys.* **251** 181–203
[44] Logunov S L, Ahmadi T S, El-Sayed M A, Khoury J T and Whetten R L 1997 Electron dynamics of passivated gold nanocrystals probed by subpicosecond transient absorption spectroscopy *J. Phys. Chem.* B **101** 3713–9
[45] Fox M 2001 *Optical Properties of Solids* (New York: Oxford University Press)
[46] Qiu J H, Zhou P, Gao X Y, Yu J N, Wang S Y, Li J, Zheng Y X, Yang Y M, Song Q H and Chen L Y 2005 Ellispsometric study of the optical properties of silver oxide prepared by reactive magnetron sputtering *J. Korean Phys. Soc.* **46** S269–75
[47] Desarkar H S, Kumbhakar and Mitra A K 2013 One-step synthesis of Zn/ZnO hollow nanoparticles by the laser ablation in liquid technique *Laser Phys. Lett.* **10** 055903–8
[48] Ben Moshe A and Markovich G 2011 Synthesis of single crystal hollow silver nanoparticles in a fast reaction–diffusion process *Chem. Mater.* **23** 1239–45
[49] Selvakannan P R and Sastry M 2005 Hollow gold and platinum nanoparticles by a transmetallation reaction in an organic solution *Chem. Commun.* 13 1684–6
[50] Guascito M R, Filippo E, Malitesta C, Manno D, Serra A and Turco A 2008 A new amperometric nanostructured sensor for the analytical determination of hydrogen peroxide *Biosensors Bioelectron.* **24** 1057–63
[51] Hao F and Nordlander P 2007 Efficient dielectric function for FDTD simulation of the optical properties of silver and gold nanoparticles *Chem. Phys. Lett.* **446** 115–8
[52] Lee T W and Gray S K 2005 Subwavelength light bending by metal slit structures *Opt. Exp.* **13** 9652–9